18

Photoinduced charge transfer in layered 2D PbSe−MoS_2 nanostructures

© I.D. Skurlov, P.S. Parfenov, A.V. Sokolova, D.A. Tatarinov, A.A. Babaev, M.A. Baranov, A.P. Litvin

Center „Information Optical Technologies“, Laboratory „Optics of quantum nanostructures“, ITMO University
197101 St. Petersburg, Russia

e-mail: ivan.skurlov.23@gmail.com

Received September 28, 2021
Revised September 28, 2021
Accepted October 13, 2021

Semiconductor 2D nanostructures are a new platform for the creation of modern optoelectronic devices. Layered 2D PbSe−MoS_2 nanostructures with efficient photoinduced charge transfer from PbSe nanoplatelets (NPLs) to MoS_2 were created. When PbSe NPLs with short organic ligands are deposited onto a thin layer of MoS_2 NPLs, a decrease in their photoluminescence intensity and a decrease in the average photoluminescence lifetime are observed. When a layered 2D PbSe−MoS_2 nanostructure is illuminated with IR radiation, a photocurrent appears, which indicates the contribution of PbSe NPLs to the electrical response of the system. Ultrathin layers of transition metal dichalcogenides sensitized with nanostructures based on lead chalcogenides can be used in photodetectors with a spectral sensitivity region extended to the near-IR range.

Keywords: nanoplatelets, transition metal dichalcogenides, charge transfer, near infrared region.

DOI: 10.21883/EOS.2022.02.53226.2773-21

Transition metal dichalcogenides (TMD) with the chemical formula MX_2 (where M — Mo, W, Pt, etc., X — S, Se, Te) have a lamellar structure, in which the layers are connected to each other by weak van-der-Waals forces and can be easily separated from each other. When the thickness is reduced to several layers, a sharp change in the physical properties of TMD occurs. The most interesting is the transition from an indirect-gap semiconductor to a direct-gap one, which has high values of the absorption coefficient in the visible region of the spectrum. Along with the high mobility of charge carriers, these properties make ultrathin TMD layers attractive for creating nanosized optoelectronic devices [1].

Near infrared (IR) photodetectors are an important component of telecommunications, night vision, bioimaging, environmental monitoring and food control systems. To this date, the manufacture of such devices is associated with technological difficulties and high production costs, which limits their application [2]. 2D-materials based on metal chalcogenides are one of the most attractive classes of nanomaterials for development of efficient and miniature near-IR photodetectors [3,4]. To improve sensitivity of photodetectors based on TMD in the near IR range, which is necessary for detecting weak signals, IR sensitizers [5] are often used. For example, quantum dots (QD) of lead and mercury chalcogenides can act as IR sensitizers. The synergy of the properties of 0D- and 2D-nanomaterials makes it possible to optimize collection of optical radiation and transport of charge carriers [6]. For example, photodetectors, highly sensitive in the near-IR range, based on ultrathin MoS_2, WSe_2 and WS_2 layers sensitized with PbS [7–9] and PbSe QDs were obtained [10,11].

Colloidal semiconductor quantum nanoplates (NP) of metal chalcogenides (CdS, CdSe, HgTe, PbSe, etc.) are a new class of nanomaterials with a number of unique physical properties: narrow and discretely tunable bands of optical transitions, low Stokes shift, fast radiative recombination, high exciton bond energy [12,13]. The unique geometry and high absorption coefficients of NPs make it possible to consider them as a promising sensitizer for optoelectronic devices, in which they can effectively absorb optical radiation and be an energy and/or charge donor [14]. For example, high-efficiency near-IR phototransistors were fabricated based on a MoS_2 monolayer deposited from the gas phase and PbS [15] nanolayers epitaxially grown on it. However, the complexity of obtaining such structures excludes the possibility of their mass production. On the contrary, colloidal nanocrystals of various geometry and chemical composition, for example, 2D-nanostructures of TDM and NP of metal chalcogenides, have a significant technological advantage.

To implement efficient photodetector devices in the near-IR range based on colloidal NP of TDMs and metal chalcogenides, it is necessary to optimize methods for depositing their thin layers, develop surface treatment methods to reduce the distance between layers, and study energy and charge transfer processes in such structures, which determine the efficiency of devices. In this present article, layered structures are created from colloidal MoS_2 and PbSe NPs. Methods have been developed for replacing the PbSe NP ligand shell, which make it possible to minimize the distance between the layers, ensuring efficient photoinduced charge transfer. It is shown that the sensitization of MoS_2 PbSe NP layers leads to an increase in the photoresponse when the system is excited by near-IR radiation.

Experimental part

Research methods

Absorption spectra were measured using a Shimadzu UV-3600 spectrophotometer. Photoluminescence (PL) spectra were measured using an original experimental complex for detecting IR PL [16,17], the spectra were corrected using a source simulating black body radiation [18]. Lasers with wavelengths of 532 and 1064 nm were used as sources of exciting radiation. An avalanche InGaAs/InP-photodiode (Micro Photon Devices) acted as a receiver to study the PL attenuation kinetics; PL was excited by pulsed lasers with wavelengths of 532 nm (pulse duration ~ 1 ns, repetition frequency 5 kHz) and 1053 nm (pulse duration 10 ns, repetition frequency 5 kHz). Microimages of the samples were obtained using a Merlin (Zeiss) scanning electron microscope (SEM) and a Solver Pro atomic-force microscope (AFM)-M (NT- MDT).

To record the photoresponse, the samples were deposited on glass substrates with an ITO (Ossila) conductive layer forming electrodes 30 mm long with a gap of 50 μm between them. The photoresponse was recorded with a Keithley 2636B picoammeter. Current-voltage curves were taken in the range from -20 to 20 V in the dark and when excited by a LED with wavelength of 1050 nm (~ 1 mW) with forward and reverse voltage changes. This method makes it possible to detect the effect of possible asymmetry of the samples? contacts. Also, the current was recorded at a constant voltage of 20 V and periodic switching on of lighting. The illumination period was equal to the darkening period and amounted to 5 s. To eliminate the effect of drift, the measurement was started 40 s after the voltage was turned on.

Samples creation

PbSe NPs were synthesized by cation exchange from CdSe NPs with thickness of 4 monolayers [19,20]. For the synthesis of CdSe NPs, CdO (70 mg, 0.545 mmol), myristic acid (340 mg, 1.49 mmol), and 27 ml of octadecene (ODE) were loaded to a three-necked flask with volume of 50 ml, the resulting solution was degassed for 30 min. at a temperature of 100°C. At the end of this time, the flask was filled with nitrogen, the temperature increased to 285°C and maintained until complete dissolution of CdO, which was expressed in solution discoloration. Then the flask was cooled to 100°C, followed by another degassing to remove water from the reaction mixture. During this time, a selenium precursor was prepared in nitrogen atmosphere: Se powder (24 mg, 0.31 μmol) was mixed with 3 ml of ODE, after which it was exposed to ultrasound for 30 min to complete dissolution. Upon completion of repeated degassing, the Se solution was introduced into a three-necked flask at temperature of 100°C, then the solution was heated to 240°C. The NP growth was triggered by the injection of $Cd(OAc)_2 \cdot 2H_2O$ (160 mg, 0.6 mmol) at temperature of 195°C. When temperature reached 240°C, solution of SeO_2 (40 mg, 0.36 mmol) in 5 ml of ODE, prepared by stirring at 200°C until clear orange solution is formed, was added to the reaction mixture at rate of 25 ml/h for 10 min. Upon completion of the injection, the flask was cooled with a water bath. 2 ml of oleic acid (OA) were introduced after reaching temperature of 160°C. NPs were separated from the reaction mixture by adding a mixture of hexane and ethanol (3 : 1 by volume) followed by centrifugation. The precipitated NPs were redissolved in 5 ml of toluene.

To obtain PbSe NP, $PbBr_2$ (125 mg, 0.34 mmol) 14 ml of ODE and 2 ml of oleylamine (OlAm) were added to three-necked flask with volume of 25 ml, the reaction mixture was degassed at temperature of 100°C for 20 h. After this time, temperature was lowered to 80°C, and the flask was filled with nitrogen. Then there was a sharp injection of the CdSe NP solution. The cation exchange reaction continued for 7 h, after which the flask was cooled to room temperature in a water bath. The reaction mixture was transferred to a centrifuge tube containing 3 ml of toluene, 12 ml of ethanol and 1 ml of OA. NPs were precipitated by centrifugation, the supernatant was removed, and the precipitate was dissolved in tetrachlorethylene (C_2Cl_4). The absorption and PL spectra and SEM -microimages of the obtained PbSe NPs are shown in Fig. 1, *a*.

Charge transfer between nanotubes in a lamellar structure is possible at a minimum distance between nanotubes. Therefore, it is necessary to replace the original long ligand shell of OA molecules with shorter ligands. The use of short ligands makes it possible to observe charge transfer in systems of IR nanostructures and TMD NP [21]. To create lamellar structures, methods have been developed for replacing the PbSe NP ligand shell with shorter organic molecules of ethanedithiol (EDT) and 3-mercaptopropionic acid (MPA).

The shell was replaced with MPA in the following way. The stock solution of PbSe NP was centrifuged by adding isopropanol in the ratio 1 : 1 by volume at 3000 rpm for 3 min. The precipitated nanoplates were redissolved into 1 ml of octane. This NP solution was added to solution of MPA (45 μl/ml) in dimethylformamide (DMF). Stirring of the resulting two-phase solution led to the transition of NP into the polar phase, which indicated that the ligands had been replaced. The octane remaining above was removed. To remove residual OA, pure octane was added to the NP-DMF solution, followed by stirring and removal of octane. Further, the resulting solution of NP-DMF was precipitated by centrifugation at 6000 rpm for 3–5 min. For subsequent application, the precipitated NPs were redissolved in a mixture of dichlorobenzene and butylamine (5 : 1 by volume) to obtain approximately the same concentration as in the stock solution. The deposition of PbSe NP films with OA and MPA shells was carried out identically. We used the method of deposition onto a rotating substrate at speed of 2000 rpm.

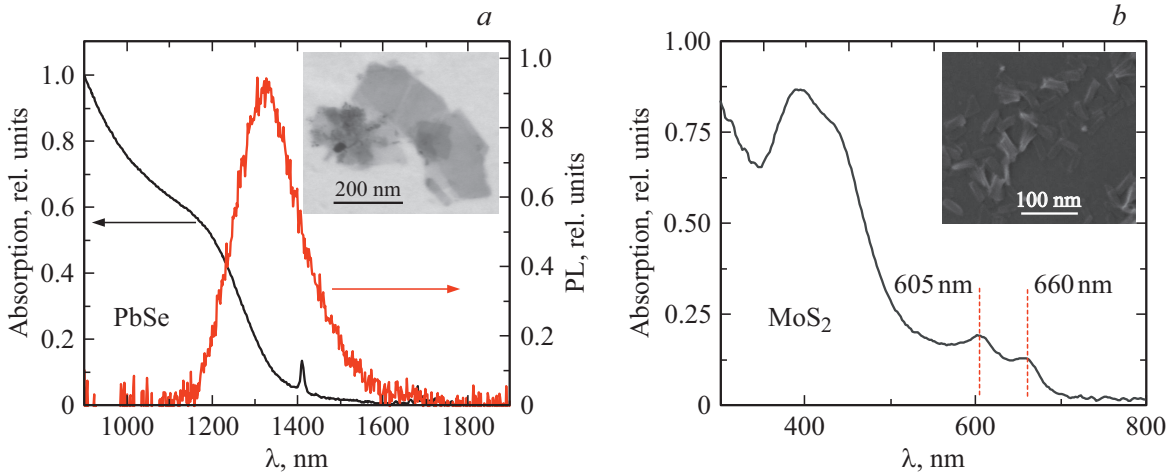

Figure 1. (*a*) Absorption (black curve) and PL (red) spectra of PbSe NP, insertion — SEM-image of PbSe NP. (*b*) Absorption spectrum of NP MoS_2, insertion — SEM-image of MoS_2 NP.

The ligand shell was replaced by EDT by layer-by-layer deposition of thin films. The initial solution for deposition of NP films with an OA shell was diluted twofold. The first layer was applied by centrifugation (2000 rpm). A solution of EDT (25 μl/ml) in acetonitrile (ACN) was dropped onto the obtained layer and hold for 40 s. After this time, the substrate was untwisted to remove the EDT solution. During untwisting (60 s) at equal time intervals ($\sim$ 10 s), the film was washed twice with pure ACN to remove excess EDT and OA and washed twice with pure hexane to increase the adhesion of the subsequent NP layer. Thus, two layers were applied.

MoS_2 NP (aqueous solution 0.1–0.5 mg/ml) were purchased from Sigma Aldrich. Prior to use, MoS_2 NPs were sequentially centrifuged at speeds of 1000, 2000 and 4000 rpm to remove aggregates. The absorption spectrum of the resulting supernatant is shown in Fig. 1, *b*. The studied MoS_2 NPs have two local absorption maxima at wavelengths of 605 and 660 nm and an intense absorption band in the spectral region 350–450 nm, which is in good agreement with the literature data [22].

Sequential centrifugation and removal of the precipitate makes it possible to exclude large aggregates from the solution and select MoS_2 NPs by lateral sizes [23]. As can be seen from Fig. 2, with a successive increase in the centrifugation speed, the average lateral size of the MoS_2 NP decreases. However, the layers obtained from the fraction with the minimum size of NP do not form a continuous film. Therefore, to create films, it was optimal to use a fraction with an average lateral NP size of $\sim$ 70 nm. For further use, MoS_2 NPs were deposited onto cleaned substrates by dropping onto a heated substrate. After drying, the substrate drops were sent to a muffle furnace heated to 280°C to remove surface stabilizer molecules. In this way, 5 layers were sequentially deposited, which ensured the formation of a thin continuous film.

Results and discussion

Figure 3 shows the PL spectra of PbSe NPs on a glass substrate and on a MoS_2 layer, normalized to the optical density of the samples. For all samples with short organic ligands (MPA, EDT), PL quenching is observed both in the presence of MoS_2 absorption (excitation at wavelength of 532 nm) and in its absence (excitation at wavelength of 1064 nm). The PL quenching in such a structure is associated with the presence of charge transfer from the PbSe NP to the MoS_2 NP layer [21].

More detailed information on charge transfer can be obtained by analyzing the PL attenuation kinetics of PbSe NPs. The PL attenuation kinetics was recorded at wavelength of 1340 nm at excitation wavelengths of 527 and 1064 nm. Approximation „of the tail“ of the PL attenuation curve was used. The cutoff time was determined at the end of the laser pulse. The PL attenuation curves upon excitation at wavelength of 1064 nm for PbSe NPs with various ligand shells deposited on a glass substrate and a thin layer of MoS_2 NPs are shown in Fig. 4. The attenuation curves were described by a biexponentially damped function, and the amplitude-averaged time was taken as the average attenuation time

$$\tau_{amp} = \frac{A_1\tau_1 + A_2\tau_2}{A_1 + A_2},$$

where A_i — amplitude and τ_i — attenuation time of the component.

The quenching efficiency was calculated using the formula

$$\eta = 1 - \frac{\tau_s}{\tau_{glass}},$$

where τ_{glass} and τ_s — PL attenuation times for PbSe NPs deposited on a glass substrate and a thin layer of MoS_2,

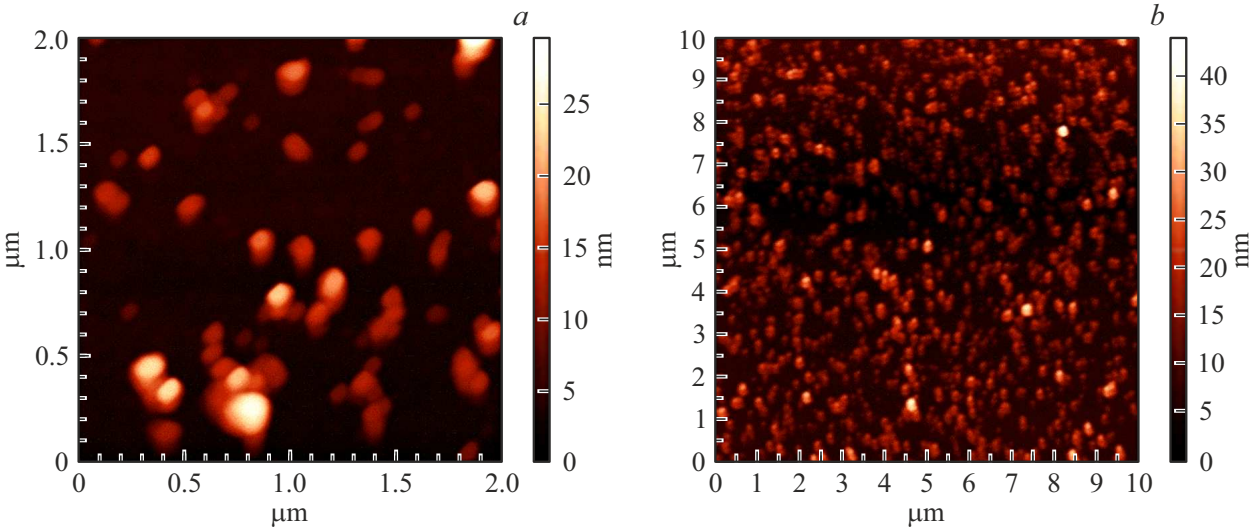

Figure 2. AFM microimages (with height scale) of MoS_2 NPs deposited at (*a*) 2000 rpm (average size ∼ 250 nm) and (*b*) 8000 rpm (average size ∼ 25 nm).

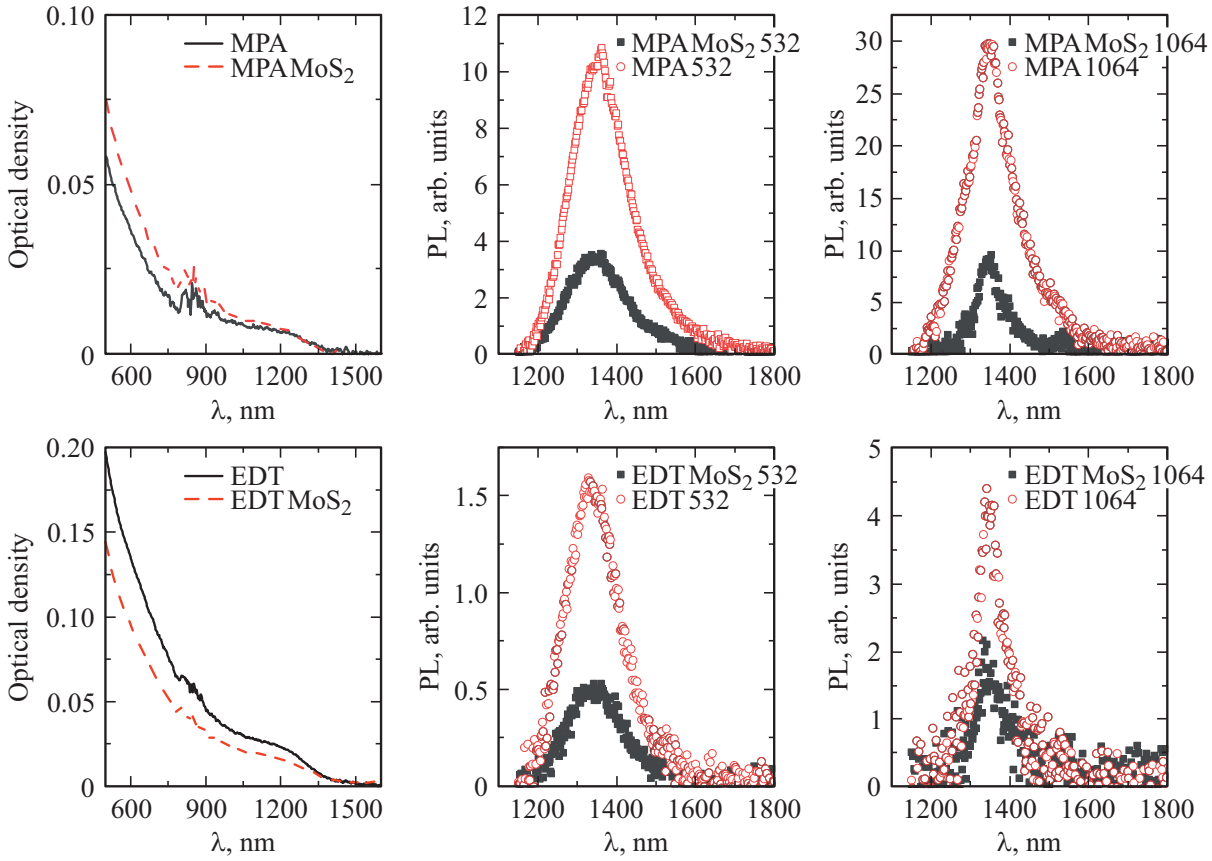

Figure 3. Absorption and PL spectra of PbSe NPs with various ligand shells deposited on a glass substrate and a thin MoS_2 NP layer.

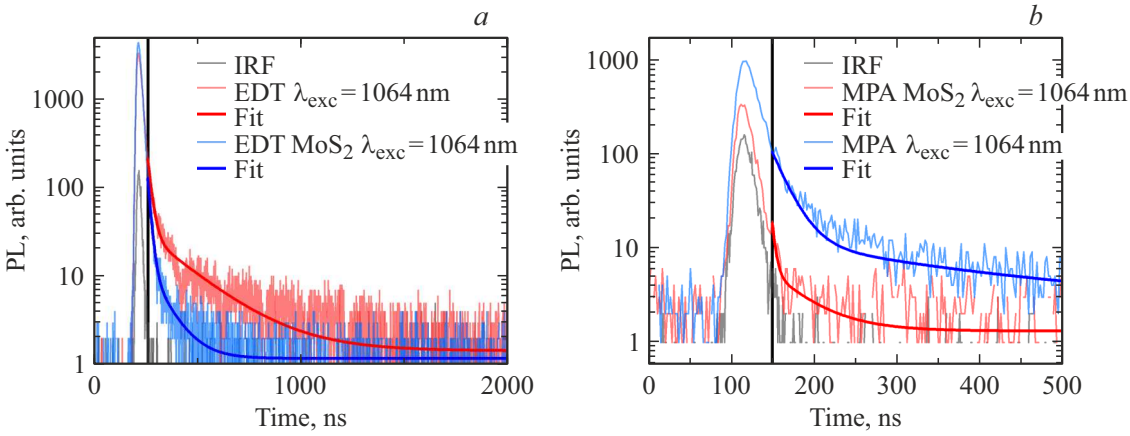

Figure 4. PbSe PL attenuation curves with EDT (*a*) and MPA (*b*) shells. The black line is the instrumental function, the red and blue lines indicate the PL attenuation curves in the absence and presence of the MoS_2 layer, respectively. The vertical line shows the cutoff after which the PL attenuation curves were approximated.

The PL attenuation times of PbSe NPs with different ligand shells deposited on a glass substrate (τ_{glass}) and a thin layer of MoS_2 (τ_s)

Shell	λ_{exc}, nm	τ_{glass}, ns	τ_s, ns	η
EDT	532	103.8	28.6	0.72
	1064	43.8	20.7	0.53
MPA	532	41.0	8.0	0.80
	1064	37.0	13.0	0.65

respectively. The calculated average PL attenuation times and charge transfer efficiencies are given in the table. It can be seen that, in both excitation regimes, more efficient quenching is observed for PbSe NPs coated with the MPA ligand shell, which is in good agreement with the ligand length: 0.4 nm for MPA and 0.6 nm for EDT. The dependence of the efficiency of charge transfer from PbS QDs to MoS_2 NPs was previously demonstrated in [21].

For lamellar 2D-nanostructures PbSe–MoS_2 deposited on ITO-substrates, the current-voltage characteristics were obtained in the dark and under LED illumination with wavelength of 1050 nm (~ 1 mW) at forward and reverse applied voltages. Figure 5 shows the current-voltage characteristics for a lamellar structure of PbSe NPs with an EDT ligand shell deposited on a MoS_2 layer (data from two photosensitive elements on the sample are given). On both photosensitive elements, the appearance of a photocurrent is observed when irradiated with light with wavelength of 1050 nm, which demonstrates the contribution of the PbSe NP to the electrical response of the lamellar structure. The insertion shows the current versus time for 2D-nanostructures PbSe–MoS_2 using EDT and MPA as ligands, demonstrating the response to light. It should be noted that a more intense photoresponse was obtained for the PbSe NP with the EDT ligand shell compared to the

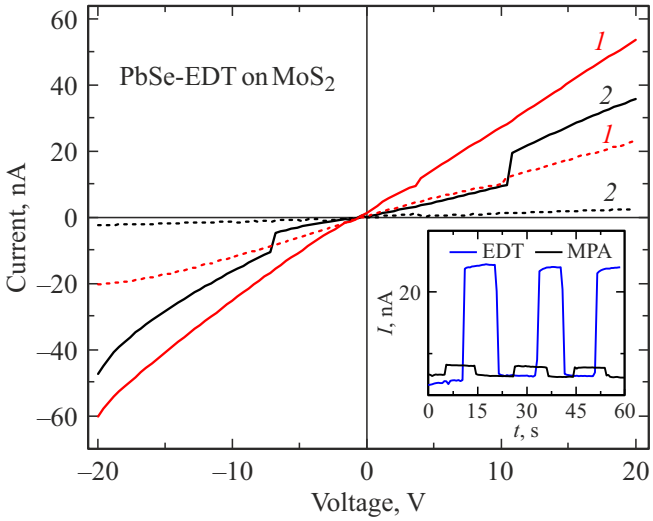

Figure 5. Current-voltage characteristics for the PbSe–MoS_2 lamellar structure with the EDT ligand shell (*1* and *2* — numbers of photosensitive elements), dashed lines — in the dark, solid lines — under IR LED illumination. Insertion — current dependences when turning on and off IR illumination.

MPA shell, which may be due to the method of formation of the PbSe NP films. The replacement of ligands by EDT molecules is carried out by the method of layer-by-layer deposition, which ensures formation of a denser NP layer.

Conclusion

Photoinduced charge transfer in lamellar 2D-nanostructures consisting of colloidal PbSe and MoS_2 nanoplates is studied. The PL quenching and reduction of the PL attenuation time of PbSe NPs upon their deposition on the MoS_2 layer were found, which indicates

the presence of photoinduced charge transfer in this lamellar structure. The most effective PL quenching is observed when shorter MPA ligands are used. The photoresponse of lamellar structures to IR radiation was found. The largest increase in the photocurrent is also observed for the film with EDT as the ligand shell, which is due to formation of a close-packed PbSe NP film.

Funding

The work was supported by the Russian Foundation for Basic Research (project 20-32-90208).

Conflict of interest

The authors declare that they have no conflict of interest.

References

[1] S. Manzeli, D. Ovchinnikov, D. Pasquier, O.V. Yazyev, A. Kis. Nat. Rev. Mater., **28** (2), 1–15 (2017). DOI: 10.1038/natrevmats.2017.33
[2] D. Yang, D. Ma. Adv. Opt. Mater., **7**, 1800522 (2019). DOI: 10.1002/ADOM.201800522
[3] F. Wang, Y. Zhang, Y. Gao, P. Luo, J. Su, W. Han, K. Liu, H. Li, T. Zhai. Small, **15**, 1901347 (2019). DOI: 10.1002/SMLL.201901347
[4] X. Zhou, X. Hu, J. Yu, S. Liu, Z. Shu, Q. Zhang, H. Li, Y. Ma, H. Xu, T. Zhai. Adv. Funct. Mater., **28**, 1–28 (2018). DOI: 10.1002/adfm.201706587
[5] C. Mu, J. Xiang, Z. Liu. J. Mater. Res., **32**, 4115–4131 (2017). DOI: 10.1557/jmr.2017.402
[6] D. Kufer, G. Konstantatos. ACS Photonics, **3**, 2197–2210 (2016). DOI: 10.1021/ACSPHOTONICS.6B00391
[7] D. Kufer, I. Nikitskiy, T. Lasanta, G. Navickaite, F.H.L. Koppens, G. Konstantatos. Adv. Mater., **27**, 176–180 (2015). DOI: 10.1002/ADMA.201402471
[8] Y. Yu, Y. Zhang, X. Song, H. Zhang, M. Cao, Y. Che, H. Dai, J. Yang, H. Zhang, J. Yao. ACS Photonics, **4**, 950–956 (2017). DOI: 10.1021/acsphotonics.6b01049
[9] C. Hu, D. Dong, X. Yang, K. Qiao, D. Yang, H. Deng, S. Yuan, J. Khan, Y. Lan, H. Song, J. Tang. Adv. Funct. Mater., **27**, 1603605 (2017). DOI: 10.1002/adfm.201603605
[10] J. Schornbaum, B. Winter, S.P. Schießl, F. Gannott, G. Katsukis, D.M. Guldi, E. Spiecker, J. Zaumseil. Adv. Funct. Mater., **24**, 5798–5806 (2014). DOI: 10.1002/ADFM.201400330
[11] B. Kundu, O. Özdemir, M. Dalmases, G. Kumar, G. Konstantatos. Adv. Opt. Mater., 2101378 (2021). DOI: 10.1002/ADOM.202101378
[12] M. Nasilowski, B. Mahler, E. Lhuillier, S. Ithurria, B. Dubertret. Chem. Rev., **116**, 10934–10982 (2016). DOI: 10.1021/acs.chemrev.6b00164
[13] E. Lhuillier, S. Pedetti, S. Ithurria, B. Nadal, H. Heuclin, B. Dubertret. Acc. Chem. Res., **48**, 22–30 (2015). DOI: 10.1021/ar500326c
[14] B. Guzelturk, H.V. Demir. Adv. Funct. Mater., **26**, 8158–8177 (2016). DOI: 10.1002/adfm.201603311
[15] Y. Wen, L. Yin, P. He, Z. Wang, X. Zhang, Q. Wang, T.A. Shifa, K. Xu, F. Wang, X. Zhan, F. Wang, C. Jiang, J. He. Nano Lett., **16**, 6437–6444 (2016). DOI: 10.1021/acs.nanolett.6b02881
[16] P.S. Parfenov, A.P. Litvin, E.V. Ushakova, A.V. Fedorov, A.V. Baranov, K. Berwick. Rev. Sci. Instrum., **84**, 116104 (2013). DOI: 10.1063/1.4829717
[17] I.D. Skurlov, D.A. Onishchuk, P.S. Parfenov, A.P. Litvin. Opt. Spectrosc., **1255** (125), 756–759 (2018). DOI: 10.1134/S0030400X18110279
[18] P.S. Parfenov, A.P. Litvin, A.V. Baranov, A.V. Veniaminov, E.V. Ushakova. J. Appl. Spectrosc., **78**, 433–439 (2011). DOI: 10.1007/s10812-011-9474-1
[19] T. Galle, M. Samadi Khoshkhoo, B. Martin-Garcia, C. Meerbach, V. Sayevich, A. Koitzsch, V. Lesnyak, A. Eychmüller. Chem. Mater., **31**, 3803–3811 (2019). DOI: 10.1021/acs.chemmater.9b01330
[20] I. Skurlov, A. Sokolova, T. Galle, S. Cherevkov, E. Ushakova, A. Baranov, V. Lesnyak, A. Fedorov, A. Litvin. Nanomaterials, **10**, 1–14 (2020). DOI: 10.3390/nano10122570
[21] I.D. Skurlov, A.S. Mudrak, A.V. Sokolova, S.A. Cherevkov, M.A. Baranov, A. Dubavik, P.S. Parfenov, A.P. Litvin. Opt. Spectrosc., **128** (8), 1236–1240 (2020). DOI: 10.1134/S0030400X20080330
[22] A. Castellanos-Gomez, J. Quereda, H.P. Van Der Meulen, N. Agraït, G. Rubio-Bollinger. Nanotechnology, **27**, 1–16 (2016). DOI: 10.1088/0957-4484/27/11/115705
[23] C. Backes, B.M. Szydłowska, A. Harvey, S. Yuan, V. Vega-Mayoral, B.R. Davies, P.L. Zhao, D. Hanlon, E.J.G. Santos, M.I. Katsnelson, W.J. Blau, C. Gadermaier, J.N. Coleman. ACS Nano, **10**, 1589–1601 (2016). DOI: 10.1021/acsnano.5b07228